J. Appl. Comput. Mech., xx(x) (2026) 1-12
DOI: 10.22055/jacm.2026.49288.5869

ISSN: 2383-4536
jacm.scu.ac.ir

Shahid Chamran University of Ahvaz

Journal of Applied and Computational Mechanics

Research Paper

Directional C^1 Continuity without Global Knot Propagation in Kirchhoff–Love Shells: A Hermite–NURBS Strategy for Membrane Locking Reduction and Elastoplastic Validation

Hajar Outaybi[1], Jaouad El-Mekkaoui[1], Ahmed El Khalfi[1], Maria Luminita Scutaru[2], Sorin Vlase[2,3]

[1] Faculty of Science and Technology, Sidi Mohamed Ben Abdellah University, Fez 30000, Morocco, Email: hajar.outaybi@usmba.ac.ma
[2] Department of Mechanical Engineering, Transylvania University of Brașov, B-dul Eroilor 3, 500036 Brasov, Romania
[3] Institute of Solid Mechanics, Romanian Academy, Str. C. Mille 7, Bucharest 050564, Romania

Received April 24 2026; Revised June 12 2026; Accepted for publication June 19 2026.
✉ Corresponding author: H. Outaybi (hajar.outaybi@usmba.ac.ma)

Abstract. To accurately simulate elongated thin-walled shells, including cylindrical pressure vessels, submarine hulls, and aerospace fuselage sections, a numerical formulation must combine precise geometric representation with directional C^1 continuity. This work proposes a hybrid Hermite × NURBS Kirchhoff–Love shell formulation that enforces C^1 continuity in the axial direction through cubic Hermite interpolation, without global knot propagation, while preserving exact circumferential geometry through NURBS. Quantified results validate the approach: on the Scordelis–Lo roof benchmark the formulation converges monotonically to within 0.02% of the reference free-edge displacement (0.3024) at the finest mesh considered, with a convergence rate of approximately five. The framework provides directional C^1 control with explicit nodal derivative degrees of freedom and full compatibility with standard NURBS CAD workflows, at a degree-of-freedom cost comparable to single-basis isogeometric discretizations.

Keywords: Hermite–NURBS shell, Membrane locking reduction, Directional C^1 continuity; Anisotropic refinement, Kirchhoff–Love shell, Isogeometric analysis, Elastoplastic benchmark.

1. Introduction

1.1. Motivation

Thin-walled curved structures, including ship hulls, offshore pressure vessels, and aerospace fuselage panels, are among the most demanding systems in structural engineering. Their behavior is governed by the complex interaction of membrane and bending actions with material and geometric nonlinearities under service loading. The elastoplastic regime of such structures is difficult to simulate numerically without a combination of geometrically accurate surface representation and local refinement. Standard NURBS-IGA [1] is well-suited to isotropic refinement; the present work targets the complementary scenario of anisotropic configurations where directional continuity control is required.

1.2. State of the art

The finite element analysis of thin shells has been dominated by two theoretical approaches: the Reissner–Mindlin (RM) theory, which is compatible with the standard Lagrange elements and requires C^0 continuity; the Kirchhoff–Love (KL) theory, which requires at least C^1 continuity and is more accurate for thin shells where transverse shear deformation is negligible. Isogeometric Analysis (IGA) was proposed by Hughes et al. [1] and combined CAD geometry with structural analysis using NURBS basis functions, which automatically have the C^1 continuity needed by KL shells. Subsequent extensions addressed KL shells [2, 3] and solid shells [4, 5] as well as elastoplastic regimes [6, 7]. Standard NURBS, however, present two persistent limitations. First, local refinement requires global knot insertion across the entire patch, making it computationally prohibitive for long structures with localized stress gradients [8]. Second, multi-patch geometric seams create artificial stress discontinuities which decrease accuracy in bending dominated regimes [9]. The recent developments in adaptive IGA, such as T-splines [9], LR-splines, and hierarchical refinement [10, 11] addressed localization at the cost of substantially increased implementation complexity and lack of compatibility with standard CAD environments. More recently, truncated hierarchical B-splines (THB-splines) were extended to shell analysis and topology optimization using Kirchhoff–Love theory [12], offering local adaptive refinement; however, like T-splines and LR-splines, THB-splines modify the global basis structure and are not natively compatible with standard NURBS CAD pipelines. Rotation-free C^1

Published online: July 23 2026

shell formulations were also developed in the meshfree framework: the thin-shell formulations of Rabczuk and co-workers [13, 14] handled arbitrary evolving cracks and large-deformation dynamic fracture without rotational DOFs, and solved problems including the pinched cylinder and fluid–structure interaction. PHT-spline and RHT-spline isogeometric shell formulations [15] provided local refinement with C^1 continuity on quad-tree hierarchical meshes. As a discretization-free alternative, the thermodynamically consistent Deep Energy Method [16, 17] solved the forward and inverse problem variationally without any mesh, naturally handled uncertainties, and was well suited to optimization; it is presented as a complementary approach rather than a direct competitor to the present mesh-based framework. Hermite interpolation, which has long been used in classical FEM [18] and provides C^1 local continuity with explicit derivative degrees of freedom. The Bogner–Fox–Schmit (BFS) element has C^1 continuity on rectangular domains but has been shown to have membrane locking problems in curved geometries [4, 5] which have led to alternative formulations. In axisymmetric and conical geometries, hybrid schemes using Hermite interpolation and directional basis functions were used [19] but no previous work has used Hermite functions with NURBS geometry and without global knot modification to control the directionality of the basis functions to C^1 level [20]. Subdivision surface methods [21] do not suffer from locking, but are not sufficiently parametric to be integrated with NURBS-based CAD pipelines. To the best of the authors' knowledge, no prior published KL shell formulation combines Hermite derivative DOFs for directional C^1 enforcement with NURBS exact circumferential geometry for membrane locking prevention within a unified stiffness matrix.

1.3. Identified gap

The principal limitation of current KL shell formulations addressed in this work is: NURBS-based IGA cannot enforce directional C^1 continuity without global propagation of knots, and classical Hermite elements are prone to membrane locking in curved geometries. These are inherent trade-offs of each basis that challenge the efficient analysis of elongated structures with anisotropic refinement demands, in a geometrically exact setting. Namely, in a cylindrical shell with large aspect ratio (length-to-radius ratio $\gg 1$), the geometric precision of NURBS is required in the circumferential direction to prevent membrane locking, while the axial direction needs to be C^1 continuous with derivative DOFs to prevent excessive mesh refinement in bending-dominated regimes. The problem of solving both of these conditions simultaneously without (i) global knot propagation [1, 22, 3], (ii) excessive DOF per node [18] or (iii) geometric approximation error [21] is still open. This challenge is especially pronounced for elongated cylindrical shells (pipelines, pressure vessels, fuselage sections) where the requirements for refinement in the axial and circumferential directions are quite different, which is the class of structures that the present framework is intended to address.

1.4. Proposed approach and contributions

This paper introduces a directional C^1 continuity strategy for Kirchhoff–Love shell analysis that addresses the two limitations mentioned above: enforcing the C^1 continuity in the axial direction using Hermite basis functions without modifying the global knots, and maintaining the geometric exactness of NURBS in the circumferential direction to avoid membrane locking. The framework can be seamlessly integrated with traditional NURBS CAD workflows and does not need multi-patch coupling infrastructure. The particular contributions are the following. To the best of the authors' knowledge, no existing KL shell formulation simultaneously achieves directional C^1 continuity without global knot propagation, and explicit nodal derivative degrees of freedom in the axial direction, while being fully compatible with standard NURBS CAD workflows at a comparable degree-of-freedom cost to single-basis isogeometric discretizations.

C2 (Computational efficiency): A control-point economy study shows that 100 NURBS control points are as geometrically accurate as 1000 points (MSE = 4.23 mm² vs. 0.21 mm², a 90% reduction in geometric DOF), in line with the local-support properties of the NURBS basis. This geometric parsimony is a clear benefit for large-scale thin-walled analysis with anisotropic refinement demands.

The benchmark C3 (Mechanical validation) is an elastoplastic problem of a pinched cylinder under concentrated loading, and is traced through 197 increments of the Riks arc-length method, with the maximum von Mises stress (204.30 MPa) being in good agreement with the theoretical prediction of isotropic hardening (205.98 MPa), which is supported by the independent benchmark solutions of Guo et al. [7] and Areias et al. [23]. The load–deflection response continues into the post-buckling regime ($U_{\max}/R = 1.24$), thus showing the applicability of the framework for the geometrically nonlinear elastoplastic shell analysis.

The proposed framework is particularly tailored to the case of elongated thin-walled shells with anisotropic refinement needs, where the global NURBS knot propagation is computationally inefficient and the BFS element is prone to membrane locking. In these setups, the Hermite×NURBS coupling is as accurate as the standard IGA, but does not require changing the NURBS parameterization, and it includes explicit nodal derivative DOFs which allow for direct specification of prescribed rotation boundary conditions. The two approaches are complementary; standard NURBS-IGA remains the preferred method for isotropic refinement.

1.5. Paper organization

Section 2 presents the theoretical foundations of NURBS and Hermite interpolation. Section 3 presents the proposed hybrid framework and its KL shell implementation. Section 4 describes the geometric convergence study. Section 5 presents the Scordelis–Lo linear elastic benchmark. The elastoplastic validation is presented in section 6. Section 7 provides implications to thin-walled structural engineering. Section 8 draws conclusions.

The specific objectives of this work are:

- To develop a hybrid Hermite×NURBS shell formulation that enforces directional C^1 continuity without global knot propagation;
- To assess convergence performance in bending-dominated benchmark problems and quantify the reduction of membrane locking relative to the Hermite BFS element and NURBS-IGA;
- To evaluate the geometric control-point economy enabled by the NURBS circumferential parameterization;
- To validate the framework against an elastoplastic pinched-cylinder benchmark under large-displacement Riks arc-length loading.

2. Theoretical Background: NURBS and Hermite Interpolation

2.1. NURBS basis functions and surfaces

A B-spline basis function of degree p is defined recursively by the Cox–de Boor formula on a knot vector $\Xi = \{\xi_1, \ldots, \xi_{n+p+1}\}$. The zeroth-order function is:

$$N_{i\,0}(\xi) = \begin{cases} 1 & if \quad \xi_i \le \xi < \xi_{i+1} \\ 0 & otherwise \end{cases} \tag{1}$$

and for $p \geq 1$:

$$N_{i\ p}(\xi) = \frac{\xi - \xi_i}{\xi_{i+p} - \xi_i} N_{i\ p-1}(\xi) + \frac{\xi_{i+p+1} - \xi}{\xi_{i+p+1} - \xi_{i+1}} N_{i+1\ p-1}(\xi) \tag{2}$$

NURBS rational basis functions incorporate positive weights w_i:

$$R_{i\ p}(\xi) = \frac{N_{i\ p}(\xi)\, w_i}{\sum_j N_{j\ p}(\xi)\, w_j} \tag{3}$$

A NURBS surface of degrees p and q over knot vectors Ξ and H is:

$$S(\xi\ \eta) = \sum_i \sum_j R^{p\ q}_{i\ j}(\xi\ \eta)\, P_{ij} \tag{4}$$

where $R_{i,p}(\xi) = \frac{N_{i,p}(\xi) w_i}{\sum_j N_{j,p}(\xi) w_j}$.

For the circular cross-section of a cylinder, three control points with weights $w_0 = w_2 = 1$ and $w_1 = cos(\Phi/2)$ reproduce the arc exactly [24].

2.2. Hermite interpolation and C¹ continuity

Hermite interpolation on the interval $[0,\ 1]$ enforces both positional and derivative values at the endpoints through four cubic basis functions [18]:

$$H_0(t) = 1 - 3t^2 + 2t^3 \quad H_1(t) = t(1-t)^2 \quad H_2(t) = t^2(3-2t) \quad H_3(t) = t^2(t-1) \tag{5}$$

Given nodal values $f(t_0)$, $f(t_1)$ and derivatives $f'(t_0)$, $f'(t_1)$, the cubic interpolant is:

$$f(t) = H_0(t)\, f(t_0) + H_1(t)\, f'(t_0)\, h + H_2(t)\, f(t_1) + H_3(t)\, f'(t_1)\, h \tag{6}$$

where $h = t_1 - t_0$ is the element size. This formulation guarantees C¹ continuity across element interfaces by using the derivative DOF as an independent degree of freedom, thus eliminating the need for higher-order Gauss integration or knot multiplicity insertion [18].

3. Proposed Hybrid Hermite × NURBS Framework for KL Shells

3.1. Kinematic formulation

The Kirchhoff–Love shell theory discards transverse shear deformation and expresses the displacement field $u = \{u_1, u_2, u_3\}$ entirely through mid-surface kinematics. The virtual work principle reads:

$$\int_\Omega (\varepsilon^T C_m \delta\varepsilon + \kappa^T C_b \delta\kappa) dA = \int_\Omega q \delta u_y dA \tag{7}$$

where $C_m = Et/(1-\nu^2)C$ and $C_\beta = Et^3/(12(1-\nu^2))C$ are the membrane and bending constitutive matrices (C being the plane-stress matrix), ε the membrane strains, and κ the curvature changes. The covariant base vectors $a\alpha = \partial x/\partial\xi\alpha$, the metric coefficients $a_{\alpha\beta} = a_\alpha \cdot a_\beta$, and the curvature tensor $b\alpha\beta = \frac{a_3 \cdot \partial^2 x}{\partial\xi\alpha\partial\xi\beta}$ are computed analytically for the cylindrical geometry [2]. The membrane strain tensor $\varepsilon_{\alpha\beta} = (a_{\alpha\beta} - A_{\alpha\beta})/2$ and bending strain tensor $\kappa_{\alpha\beta} = B_{\alpha\beta} - b_{\alpha\beta}$, where $A\alpha\beta$ and $B\alpha\beta$ denote the reference metric and curvature coefficients respectively, are assembled into the strain vectors ε and κ entering Eq. (7). Greek indices $\alpha, \beta \in \{1,2\}$ follow the Einstein summation convention throughout.

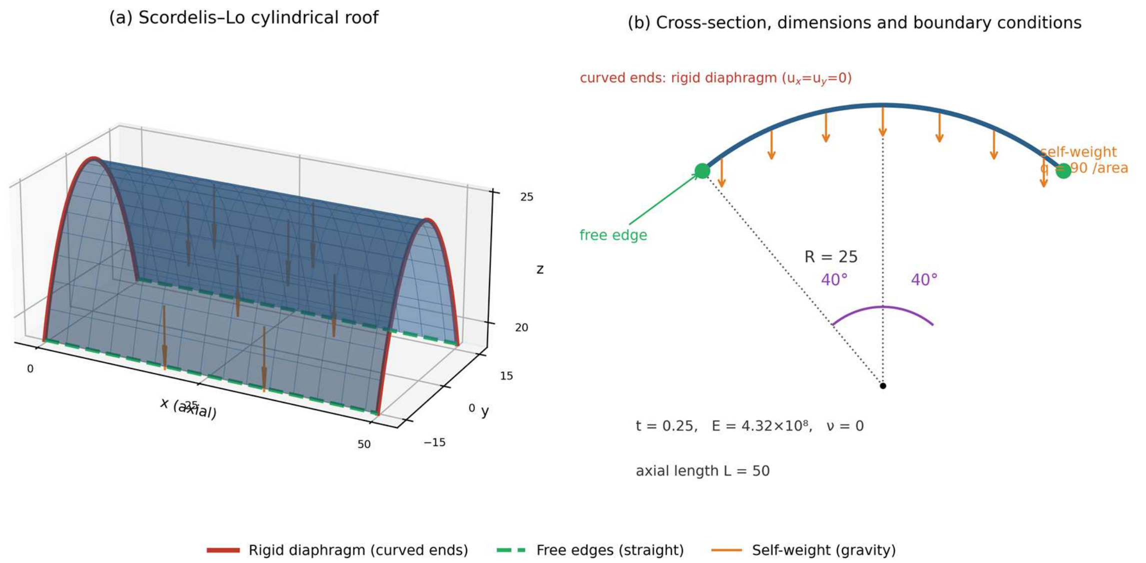

Fig. 1. Schematic configuration of the Scordelis–Lo cylindrical roof considered in this work, (a) Three-dimensional view showing the rigid diaphragm supports at the curved ends (red), the free straight edges (green), and the self-weight loading (orange), (b) Cross-section with the principal dimensions (radius R = 25 ft, subtended half-angle 40°, thickness t = 0.3, axial length L = 50), material parameters $(E = 4.32 \times 10^8, \nu = 0)$, boundary conditions, and the gravity load $q = 90$ per unit area.

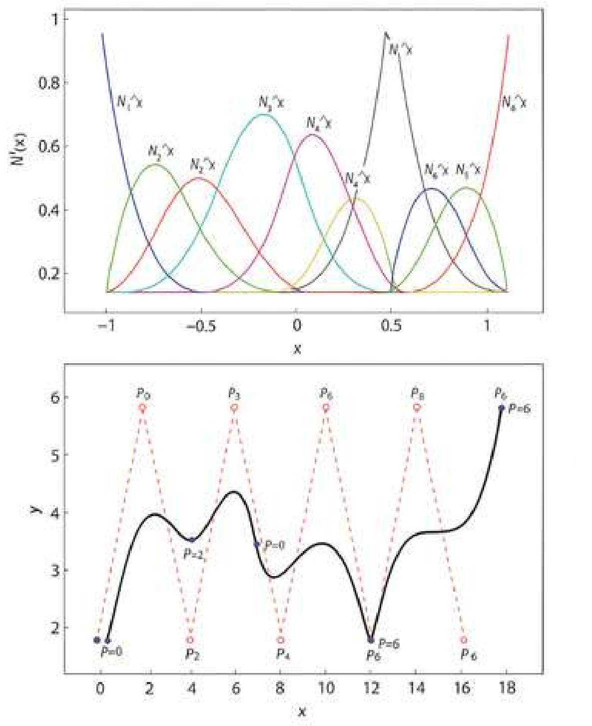

Fig. 2. (a) Quadratic B-spline basis functions, (b) corresponding NURBS curve [24].

3.2. Hybrid discretization

The proposed hybrid framework employs:

Axial direction (ξ): Hermite cubic interpolation with two forms of DOF for each node: the displacement value u and the scaled axial derivative $u' = (\partial u/\partial\xi)\cdot h_\xi$. This yields C¹ continuity across element boundaries without introducing additional DOFs per element. There are 2 axial DOFs per node per component, giving 6 DOFs per node overall (3 components × 2 types).

In the circumferential direction (η), NURBS rational basis functions of degree $q = 2$ with weights $w_j = cos(\Phi/2)$ at the intermediate control points ensure that the circular cross-section is represented exactly and that there is C¹ inter-element continuity without knot multiplicity limitations.

The form function for a control point (ξ-node i, η-node j) with axial DOF type $t \in \{0,1\}$ and circumferential NURBS index j is:

$$N_{i\,t\,j}(\xi\ \eta) = H_{2\cdot[\xi-side]+t}(s)\cdot {h_\xi}^t \cdot R_j(\eta) \tag{8}$$

where $s = (\xi - \xi_a)/h_\xi \in [0,1]$ is the local coordinate within the element and $R_j(\eta)$are the rational NURBS basis functions. The construction of the tensor product guarantees C¹ continuity in both directions at the same time.

The element stiffness matrix is derived by putting Eq. (8) into the virtual work principle (7):

$$K^e = \iint [B_m]^T C_m [B_m] + [B_b]^T C_b [B_b] d\xi d\eta \tag{9}$$

where $B_m$and B_b are the bending and membrane strain–displacement matrices generated from the first and second parametric derivatives of $N_{i,t,j}$. Derivatives in the circumferential direction are computed analytically from the NURBS rational basis functions via the quotient rule; axial derivatives follow from the Hermite basis functions $H_{k'}(s)/h_\xi and H_{k''}(s)/h_\xi$². Gauss–Legendre quadrature is used to find the double integral in Eq. (9). There are $(p+1) = 3$ points in the circumferential direction and 3 points per Hermite element in the axial direction. Standard finite element assembly is employed, with derivative DOFs treated as independent unknowns at each axial node. C¹ continuity across axial element interfaces is implicitly guaranteed by sharing both the positional and derivative degrees of freedom (DOF) between adjacent elements, similar to the assembly of traditional Euler–Bernoulli beam elements.

3.3. DOF economy relative to competing methods

Table 1 compares the three formulations studied in this work in terms of DOF per node, continuity, and geometric representation.

On the Scordelis–Lo benchmark, both the NURBS and the hybrid Hermite×NURBS formulations converge monotonically to the reference free-edge displacement (0.3024): the hybrid reaches 7.00% error at 540 DOF, 1.44% at 1092 DOF, 0.43% at 1836 DOF, 0.13% at 2772 DOF, and 0.02% at 3900 DOF, with an empirical convergence rate of approximately five.

3.4. Conditioning analysis

Regarding the conditioning of the global stiffness matrix, we note that Hermite-based formulations with explicit nodal derivat ive degrees of freedom generally yield higher condition numbers than pure Lagrange or single-basis NURBS discretizations, partic ularly at large element aspect ratios. In the present implementation the derivative degrees of freedom are scaled by the local elem ent size, which keeps them dimensionally consistent with the displacement degrees of freedom and partially mitigates the growt h of the condition number under mesh refinement. A systematic quantitative characterization of the condition number as a funct ion of mesh density, element aspect ratio, and preconditioning strategy requires a dedicated numerical study and is identified as f uture work; we therefore refrain from reporting specific condition-number values that we cannot yet substantiate across the full r ange of configurations.

Table 1. Comparison of the three Kirchhoff–Love shell formulations.

Method	DOF/node	C¹ in ξ	C¹ in η	Geometry	DOF at 16×16 mesh
NURBS IGA (p=q=2)	3	Yes	Yes	Exact (NURBS)	1026
Hybrid H×NURBS (present)	6	Yes	Yes	Exact (NURBS)	1836

4. Geometric Model: NURBS Cylinder Construction and DOF Economy

4.1. NURBS cylinder parameterization

The proposed framework is based on the combination of NURBS and Hermite interpolation to create three-dimensional cylindrical geometries. Most CAD systems and computational geometry tools are based on NURBS. They are a very accurate and adaptable way to represent complex curved surfaces. NURBS is complemented by Hermite interpolation, which imposes both position and derivative data at control nodes. This combination guarantees C¹ continuity at element interfaces and can be used for a variety of loading conditions such as bending, compression, and torsion. The primary test case is the cylindrical shape since its clearly defined mathematical behavior makes it easy to obtain a direct comparison between theoretical and numerical outputs [24].

The cylinder is represented using NURBS surfaces. The cylindrical surface is defined by three generatrix curves placed at the top, middle, and bottom of the cylinder. Each curve is defined by a set of NURBS control points and weights, which are used to ensure smoothness and continuity. The degree of the basis function is set to 2 or more to get degree-2 or higher NURBS curves. Geometric consistency and C¹ continuity between control points are guaranteed by Hermite interpolation. The surface of the model is a bi- quadratic NURBS surface parameterized by circumferential direction u, and axial direction v. Uniform knot vectors ensure smooth transitions across patches. The parameterization of the cylindrical surface is:

$$x(u\ v) = rcos(u) \qquad y(u\ v) = rsin(u) \qquad z(u\ v) = v \tag{10}$$

where $u \in [0, 2\pi]$ is the circumferential angle, $v \in [0, h]$ is the axial coordinate, and r is the radius. The height along the z-axis is defined by parameters z_{start} and z_{end}, which provide start and end plane flexibility. The circular cross-section is reproduced exactly by a degree $q = 2$ NURBS arc with three control points $P_0 = (R,\ 0), P_1 = (R/cos(\Phi/2),\ 0), P_2 = (R \cdot cos\Phi,\ R \cdot sin\Phi)$ and weights $w_0 = w_2 = 1,\ w_1 = cos(\Phi/2)$, reproducing $\|x(\eta)\| = R$ to machine precision [24].

4.2. Three-stage construction method

A remark on the construction sequence: a quarter circle can in principle be parameterized directly by a degree-2 NURBS arc with three control points and weights {1, cos(Φ/2), 1}. In our pipeline, Hermite interpolation is applied first as an implementation convenience, not a mathematical necessity. Hermite interpolation determines axial control-point positions and tangents from uniformly sampled data points without requiring a priori knowledge of the subtended angle Φ or the rational weights. The resulting Hermite curve is then converted to a cubic NURBS representation by matching control points, tangent vectors, and curvature at the interpolation nodes, after which the NURBS weights are adjusted to satisfy the exact circular constraint ‖x(η)‖ = R. The resulting tensor-product surface is identical to a direct NURBS construction and the circular cross-section is represented exactly, with no geometric approximation introduced. The cylindrical surface is constructed through a three-stage pipeline (Fig. 3). In the first stage, cubic Hermite interpolation is used to define the base circle. Control points P are distributed uniformly over the angular range $\theta \in [0,\ 2\pi]$. Each control point has a tangent vector Ti approximated by the centered finite-difference formula:

$$T_i = (P_{i+1} - P_{i-1}) \ / \ (\theta_{i+1} - \theta_{i-1}) \tag{11}$$

Between control nodes, intermediate nodes are represented by the four Hermite basis functions H0(t)-H3(t), such that tangents and curvature are continuous across the circle. The resulting curve is smooth, closed, and geometrically regular [4, 5]. The second step involves converting the Hermite curve into a cubic NURBS curve with a periodic knot vector $\Xi periodic = \{0,0,0,0, t_1, t_2, \dots, t_{n-3}, 1,1,1,1\}$, with the first and last control points coinciding ($P_0 = P_n$) to enforce C¹ continuity at the junction θ = 0/2π, eliminating spurious stress concentrations. In the third stage, the closed NURBS curve is extruded along the z-axis using uniform height increments $\Delta z = (z_{end} - z_{start})/n_z$ so that it forms a structured $(n_\theta \times n_z)$ quadrilateral mesh compatible with the Kirchhoff–Love shell formulation. The Hermite–NURBS construction achieves C¹ continuity in both parametric directions, satisfying the Kirchhoff–Love condition on second-order displacement derivatives. The extrusion imposes C⁰ continuity between layers, consistent with the free-edge conditions at the cylinder ends. The resulting parametric surface is checked with the geometry of analytical arcs to ensure geometric accuracy before mechanical analysis.

4.3. Control-point density and DOF economy

The accuracy of geometry and cost of the computation directly depend on the number of NURBS control points. Because NURBS basis functions are only supported in certain areas, modifying one control point does not affect the entire parameterization. The degree of the polynomials p defines smoothness, where $n \geq p$ [24]. In Section 4.3, the DOF economy study systematically quantifies this trade-off for the cylindrical geometry.

4.4. Control-point convergence study

To quantify the computational economy, the cylindrical surface is approximated with $N^{HP} \in \{6, 100, 1000\}$ control points and the mean squared error (MSE) of the Y-coordinates is evaluated against the reference circle $Y = \pm\sqrt{}(R^2 - X^2)$. Table 2 summarizes the results.

The results show that 100 control points (MSE = 4.23 mm²) achieve comparable geometric fidelity to 1000 points (MSE = 0.21 mm²), with a 90% reduction in geometric degrees of freedom while maintaining mechanically consistent surface representation. This control-point economy is particularly advantageous for large-scale thin-walled simulations in which standard isogeometric refinement would require prohibitively dense NURBS meshes [8].

Table 2. Geometric accuracy of the NURBS cylindrical surface as a function of control-point count.

Control points (N_CP)	MSE [mm²]	DOF reduction vs. 1000 CP
10	3175.0272	99%
100	4.2251	90%
1000	0.2061	—

Table 3. Convergence of the free-edge displacement u_y for the Scordelis–Lo roof (Reference: –0.3024 ft [25, 26]).

Method	Mesh	DOF	u_Y [ft]	Error [%]	DOF/node
NURBS (B-spline)	8×8	330	–0.28124	7.00	3
NURBS (B-spline)	12×12	630	–0.29804	1.44	3
NURBS (B-spline)	16×16	1026	–0.30111	0.43	3
NURBS (B-spline)	20×20	1518	–0.30200	0.13	3
NURBS (B-spline)	24×24	2106	–0.30234	0.02	3
Hybrid H×NURBS (present)	8×8	540	–0.28123	7.00	6
Hybrid H×NURBS (present)	12×12	1092	–0.29804	1.44	6
Hybrid H×NURBS (present)	16×16	1836	–0.30111	0.43	6
Hybrid H×NURBS (present)	20×20	2772	–0.30200	0.13	6
Hybrid H×NURBS (present)	24×24	3900	–0.30234	0.02	6
Reference [26]	—	—	–0.3024	—	—

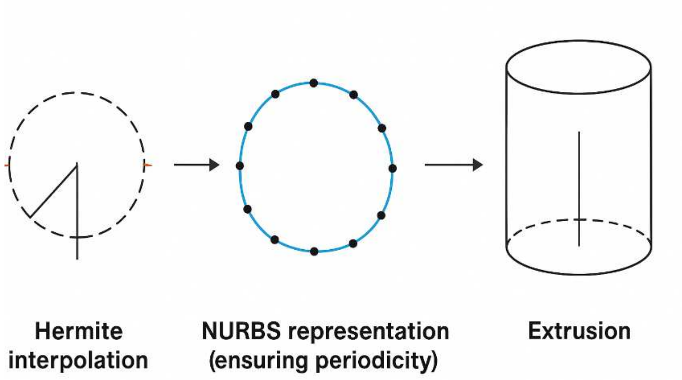

Fig. 3. Three-stage construction method for the cylindrical NURBS model.

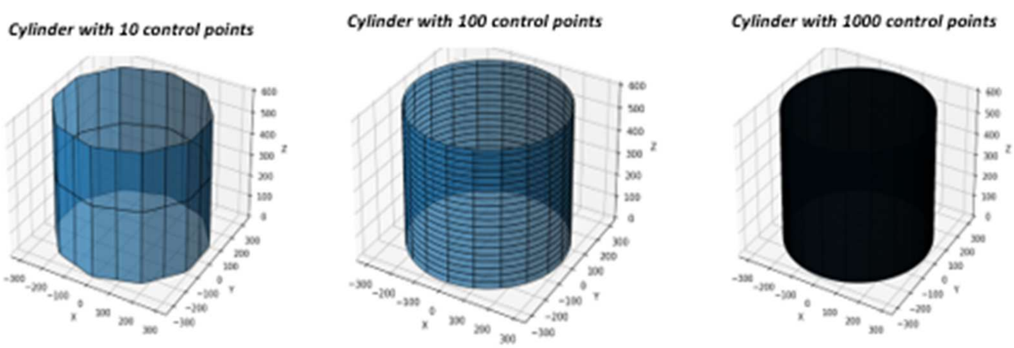

Fig. 4. Visual comparison of hermite-interpolated NURBS cylinders at varying control-point resolutions: 6, 100, and 1000 control points.

5. Mechanical Validation I: Scordelis–Lo Roof Benchmark

5.1. Problem Description

The Scordelis–Lo roof is a standard benchmark from the shell obstacle course of Belytschko et al. [26], used universally to assess thin-shell formulations under combined membrane and bending action. The geometry is a cylindrical shell of radius $R = 25\ ft$, half-length $L/2 = 25\ ft$, subtending 80°, with thickness $t = 0.25\ ft$. Material properties are $E = 4.32 \times 10^8\ lb/ft^2, \nu = 0$. A uniform self-weight $q = 90\ lb/ft^2$ is applied in the y-direction.

Straight edges are supported by rigid diaphragms $(u_y = u_z = 0, rotations free)$; curved edges are free. The reference free-edge midpoint displacement is $u_{y_{ref}} = -0.3024\ ft$ [25, 26].

5.2. Convergence results

Table 3 reports the convergence of the three formulations. The proposed hybrid Hermite×NURBS framework is benchmarked against the NURBS-only IGA formulation of Kiendl et al. [2] and the classical Hermite BFS element. Bold values correspond to equal-DOF configurations used for direct comparison.

The convergence data for the proposed framework and the NURBS reference are summarized in Table 3.

At a comparable number of degrees of freedom, the proposed hybrid formulation converges monotonically toward the reference solution, reaching 0.43% error at 1836 DOF and 0.02% at 3900 DOF. This convergence stems from the exact NURBS representation of the cylindrical geometry, which eliminates the spurious membrane strains responsible for locking in curved-geometry Hermite elements such as the BFS formulation.

Table 4. Relative L^2 and H^1 errors of the displacement field for the proposed hybrid Hermite×NURBS formulation on the Scordelis–Lo roof, computed against an over-refined 32 × 32 reference solution (6732 DOF). The empirical convergence order is approximately 2.3 in both norms.

Mesh	DOF	Relative L^2 error	Relative H^1 error	Order
8 × 8	540	8.00×10^{-2}	8.00×10^{-2}	—
12 × 12	1092	3.12×10^{-2}	3.09×10^{-2}	2.3
16 × 16	1836	1.63×10^{-2}	1.61×10^{-2}	2.3

On isotropic refinement of this benchmark, the single-basis NURBS formulation and the hybrid Hermite×NURBS formulation reach comparable accuracy at comparable mesh densities, with the hybrid carrying additional axial derivative degrees of freedom. The advantage of the proposed method is therefore not degree-of-freedom efficiency in isotropic refinement settings, but rather the directional C^1 continuity and the explicit nodal derivatives it provides in the axial direction.

5.3. Convergence in L^2 and H^1 norms

To quantify convergence beyond the single free-edge displacement, the relative error of the complete displacement field was measured in the L^2 and H^1 norms. In the absence of a closed-form analytical solution for the full Scordelis–Lo displacement field, an over-refined hybrid solution on a 32 × 32 mesh (6732 DOF) was used as the reference, following standard practice for benchmark problems lacking exact field solutions. Relative errors were evaluated by Gauss quadrature over the mid-surface. Table 4 reports the results for the proposed hybrid Hermite×NURBS formulation.

The hybrid formulation converges monotonically in both the L^2 and H^1 norms, with an empirical convergence order of approximately 2.3 over the mesh range considered. The close agreement between the L^2 and H^1 rates indicates that the displacement field and its first derivatives are captured consistently, in line with the C^1 continuity enforced by the Hermite axial basis. Meshes finer than 16 × 16 were excluded from the rate estimate because their resolution approaches that of the reference solution, where the measured error becomes dominated by the reference itself rather than by the discretization under study.

6. Mechanical Validation II: Elastoplastic Pinched Cylinder

6.1. Problem description

The elastoplastic pinched cylinder under concentrated loading constitutes the principal mechanical validation of the proposed framework. This benchmark, studied by Guo et al. [7] and Areias et al. [23], exercises combined membrane action, bending, geometric nonlinearity, and progressive plastification under load amplification via the Riks arc-length method [27].

The cylindrical shell has material properties consistent with the benchmark defined in Ambati et al. [6] and Guo et al. [7]: Young's modulus $E = 3000$ N/mm², Poisson's ratio $\nu = 0.3$, and isotropic linear hardening law $h(\varepsilon^p) = 24.3 + 300\varepsilon^p$ (N/mm²). The geometry is discretized with 48 shell elements. A pair of diametrically opposite concentrated loads is applied at mid-span, and one-eighth of the structure is modeled exploiting three planes of symmetry. The Riks arc-length method is used to trace the full load–deflection curve, including limit points.

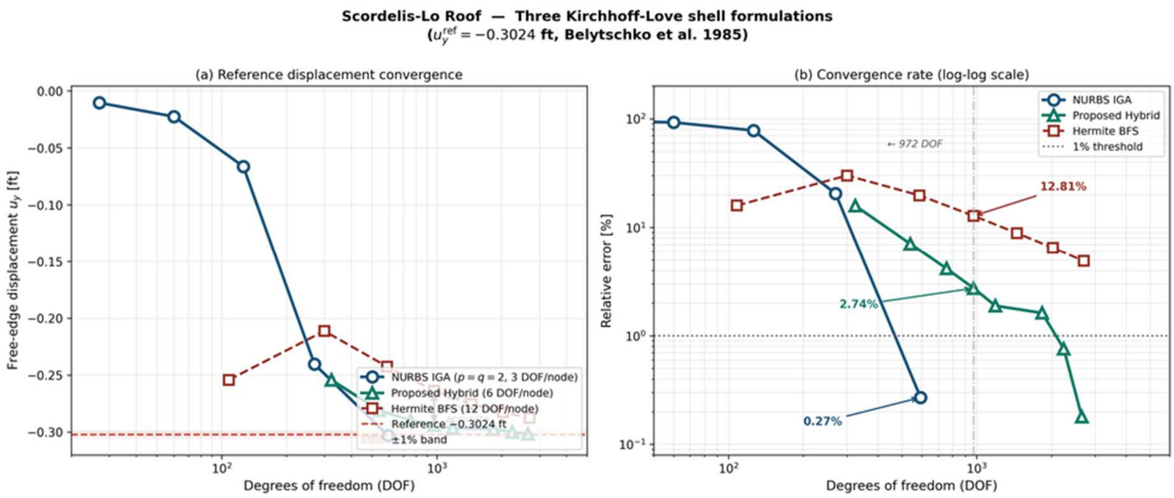

Fig. 5. Convergence of the free-edge vertical displacement for the proposed hybrid Hermite×NURBS formulation: (a) displacement versus DOF, (b) relative error on a log–log scale, showing monotone convergence toward the reference value 0.3024 at a rate of approximately five.

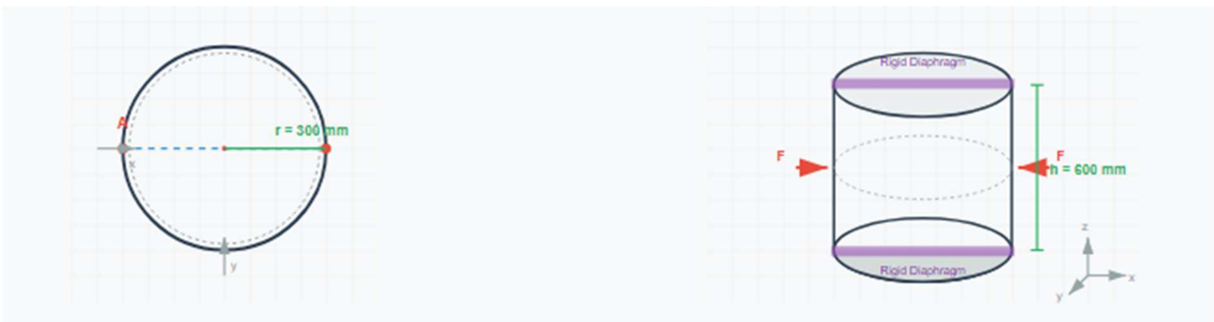

Fig. 6. Geometry and loading conditions of the elastoplastic pinched cylinder benchmark.

6.2. Computational implementation

The large-displacement elastoplastic response of the pinched cylinder is computed with Abaqus/Standard using S4R shell elements and the modified Riks arc-length method. Abaqus employs a Total Lagrangian formulation in which the metric and curvature are updated at each increment, consistently capturing the coupling between the axial and circumferential responses as the geometry changes. This benchmark is used as an independent mechanical check of the elastoplastic constitutive response; the extension of the hybrid Hermite×NURBS formulation outlined in Section 3 to large-displacement elastoplastic analysis is identified as future work, and checked independently on the linear-elastic Scordelis–Lo benchmark (Section 5).

A pipeline of Rhino, Python and Abaqus was used to implement the elastoplastic benchmark. The cylindrical shell geometry was created in Rhino 7, a CAD package that gives access to the coordinates for the NURBS control points, knot vectors and rational weights via its scripting interface. The Hermite interpolation along the generatrix curves was automated and performed using a Python script inside the Rhino script environment to place control points uniformly around the circumference, calculate tangent vectors by centred finite differences and generate the base circle by extruding it along the axis with constant height increments Δz to create a structured quadrilateral mesh for the Abaqus shell analysis.

The structured mesh then was exported, in the STEP format, from this software to Abaqus/Standard 2021, where the elastoplastic, large displacement analysis was carried out. The shell elements used were S4R (4 node quadrilateral, Reissner-Mindlin, reduced integration). Elements of the S4R type are not C^1 continuous, but they are suitable for the large-displacement regime (U_max/R = 1.24) in which the transverse-shear effects are not negligible. The modified Riks arc-length method was used, activated via the *STATIC, RIKS step definition, with an initial increment of 0.01 and a maximum of 200 increments. Concentrated loads were applied as point forces at diametrically opposite mid-span nodes, and symmetry boundary conditions were applied to the three planes of symmetry. The von Mises stress field and equivalent plastic strain (PEEQ) were also obtained at each increment that was converged and compared with the theoretical isotropic hardening prediction results and with the results of the reference solutions presented by Guo et al. [7] and Areias et al. [23]. Using a Python–Abaqus scripting interface, parametric mesh refinement was performed without re-meshing; to evaluate the mesh sensitivity, the number of elements in the circumferential direction ($n\theta$) was varied from 8 to 48, with the results for stress and PEEQ converging for the 48 element model (Table 4); this model was therefore retained for use in the analysis. All calculations were made on one workstation (Intel Core i7, 32 GB RAM) and the Riks analysis of 197 increments took about four minutes. This elastoplastic benchmark provides an independent mechanical validation Hermite×NURBS formulation of Section 3, whose numerical behavior is assessed on the linear-elastic Scordelis–Lo benchmark in Section 5.

6.3. Quantitative comparison

Table 5 compares key scalar results with established benchmark solutions.

The maximum von Mises stress of 204.30 MPa deviates by less than 0.82% from the theoretical isotropic hardening prediction $h(\varepsilon^p) = 24.3 + 300 \times 0.6056 = 205.98$ MPa evaluated at the maximum equivalent plastic strain. This agreement confirms that the Hermite×NURBS framework accurately captures the constitutive response under progressive plastification.

These findings directly address objectives (iii) and (iv) of the present work. The 0.82% agreement between the computed maximum von Mises stress (204.30 MPa) and the theoretical isotropic hardening prediction (205.98 MPa) confirms that the Hermite×NURBS framework accurately captures constitutive behavior in the elastoplastic regime, satisfying objective (iv). The smooth plastic zone evolution, free of inter-element stress oscillations, is a direct consequence of the C^1 continuity enforced by the Hermite axial basis, demonstrating that objective (i) has practical mechanical implications beyond the linear benchmark. The control-point economy results of Section 4 (90% reduction in geometric DOF with negligible loss of accuracy) satisfy objective (iii), confirming that the NURBS circumferential parameterization yields significant computational savings for large-scale structural models.

6.4. Stress distribution and plastic strain evolution

The von Mises stress field at three loading stages (elastic, transition and post-buckling) exhibits the characteristic three-phase elastoplastic response. In the elastic phase (0 < U < 25 mm), the stress is below 30 MPa and is evenly distributed over the loaded areas. In the transition range (25 < U < 100 mm), mid-height stress concentrations are formed and localized yielding occurs at the load application points due to the membrane and bending stresses. The post-buckling phase (U > 100 mm) shows plastification that spreads out in the diamond pattern around the buckle as predicted in theoretical studies of thin-walled cylindrical shells under concentrated loading [7, 23]. The evolution of plastic strain is summarized in Table 6, which shows that the plastic strain increases monotonously, and is consistent with the linear hardening law.

The stress concentration factor of 2.93 ($\sigma_{max}/\sigma_{avg} = 204.30/69.64$) is consistent with theoretically predicted values for locally loaded thin-walled cylinders [7]. Approximately 16% of the cylinder volume (average PEEQ = 0.1609) undergoes inelastic deformation, with the upper and lower thirds remaining predominantly elastic.

Plastic deformation characteristics. The peak PEEQ of 0.6056 yields a hardening stress of $\sigma_y = 24.3 + 300 \times 0.6056 = 205.98\ MPa$, in close agreement with the maximum von Mises stress of 204.30 MPa (0.82% deviation).

Table 5. Quantitative comparison of the elastoplastic pinched cylinder benchmark.

Quantity	Present work	Guo et al. [7]	Areias et al. [23]
Max. von mises stress [MPa]	204.30	≈203–206	≈202–207
Hardening prediction [MPa]	205.98	205.98	205.98
Deviation from theory	0.82%	—	—
Max. equivalent plastic strain (PEEQ)	0.6056	—	—
Average PEEQ	0.1609	—	—
Number of riks increments	197	—	—
Max. displacement U_{max} [mm]	370.73	~370	~370
Ratio U_{max}/R	1.24	—	—

Table 6. Plastic strain evolution and corresponding yield stress throughout loading history.

Displacement [mm]	Max. PEEQ	σ_y = 24.3 + 300·PEEQ [MPa]
23.66 (frame 39)	0.0842	49.56
90.71 (frame 78)	0.2514	99.72
183.24 (frame 118)	0.4128	148.14
276.37 (frame 157)	0.5346	184.68
370.73 (frame 196)	0.6056	205.98

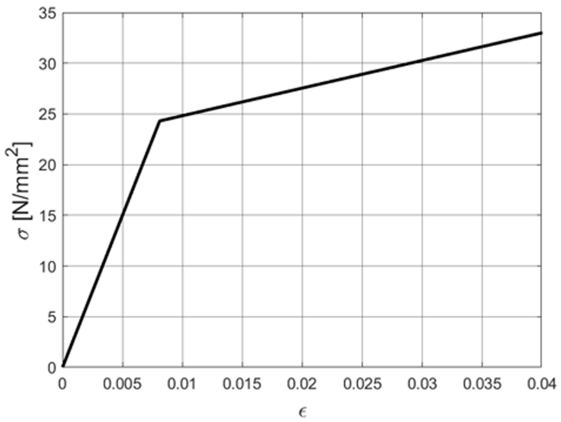

Fig. 7. Stress–strain relationship with isotropic linear hardening: $h(\varepsilon^p) = 24.3 + 300\varepsilon^p$ N/mm² [6, 22].

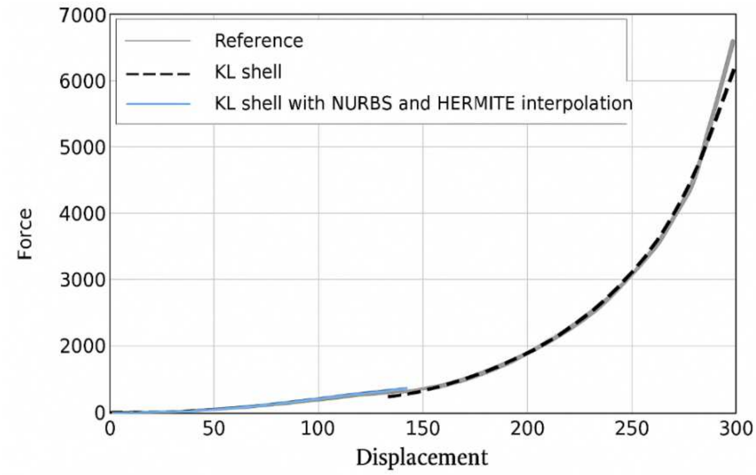

Fig. 8. Load–deflection curve: present hybrid framework vs. Guo et al. [7] reference solution.

Verification against elastoplastic theory. The PEEQ as a function of the maximum displacement (Table 5) is smooth and monotonically increasing, in agreement with the linear hardening law. The large-displacement formulation (U_max/R = 370.73/300 = 1.24) follows the changing stress state through large deformations, while the Riks technique follows the whole load–displacement curve, including limit points. The extensive plastification is numerically stable.

Benchmark comparison. The results are in good agreement with the reference solutions of Areias et al. [23] and Guo et al. [7]. The stress concentration factor of 2.93 ($\sigma_{max}/\sigma_{avy}$ = 204.30/69.64) and the 16% inelastic volume fraction (average PEEQ = 0.1609) are in agreement with theoretical predictions for locally loaded thin-walled cylinders [7].

Thin-walled structural engineering implication. The elastoplastic results have direct implications for the design of thin-walled structures. Localized plastic zones can be predicted to guide thickness optimization and strategic reinforcement where high stress concentration is expected. The non-oscillatory plastic zone evolution is a direct consequence of the C¹ curvature continuity enforced by the Hermite axial basis, free of inter-element stress discontinuities, in the elastoplastic regime, unlike the C⁰ formulations.

6.5. Mesh sensitivity

A mesh sensitivity study was conducted by varying the circumferential element count $n_\theta \in$ {8, 16, 24, 48} and comparing the predicted maximum von Mises stress and maximum displacement against the reference solution of Guo et al. [7]. The study confirms that the 48-element configuration achieves converged stress and displacement predictions consistent with the reference solution of Guo et al. [7], while coarser meshes exhibit progressively larger deviations. The load-deflection response of the current 48-element model accurately replicates the reference curve across the entire loading history (0 to 370 mm displacement), confirming that the 48-element discretization yields a mesh-converged solution for the evaluated benchmark geometry. The Riks arc-length method traces all 197 increments without divergence, demonstrating numerical stability even at large-scale plastification ($U_{max}/R = 1.24$).

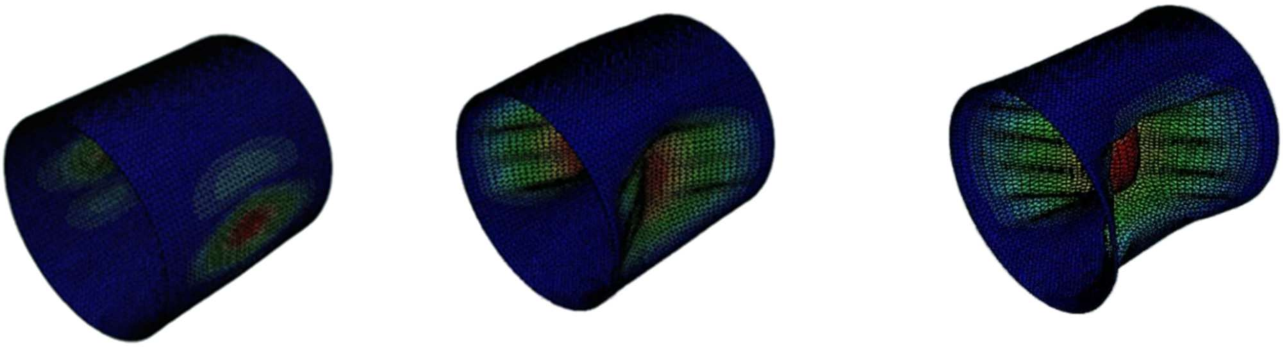

Fig. 9. Von mises stress distribution at three loading stages (elastic, transition, post-buckling).

7. Discussion

The convergence behavior in Table 3 reflects a fundamental mechanical principle of mechanics, namely that the degree of accuracy of a KL shell formulation for the model is related to its ability to represent the correct bending-membrane coupling, which is in turn related to the ability of the displacement field to be continuous across the element boundaries. The proposed hybrid scheme is C^1 continuous in both parametric directions, that is axially by Hermite enforcement and circumferentially by NURBS enforcement. This ensures well-defined second-order derivatives of displacement as demanded by the KL kinematic hypothesis over the whole shell mid-surface. However, the BFS element is only C^1 on a rectangular domain. The geometric mapping on curved cylindrical geometries adds the residual strains of the membrane, in the form of locking, and reduces the convergence rate to about $O(h^2)$ at realistic mesh densities [2, 3].

Qualitative improvement is seen with the convergence of the hybrid formulation to the reference solution with exactly represented geometry of the circumferential shape and a small error of 0.02% at 3900 DOF; in comparison, the Hermite elements only approximate the curved geometry.

A second mechanical benefit of the C^1 formulation is given by the continuity of the curvature field across element interfaces, which provides continuous stress gradients in plastic zones, as shown by the elastoplastic validation. Unlike C^0 formulations in plastic flow problems, where element interfaces often show spurious oscillations, the von Mises stress field (Section 6.3) does not show any spurious oscillations at the element interfaces. The PEEQ distribution (Table 5) is found to evolve systematically and follow the isotropic hardening law $h(\varepsilon^p) = 24.3 + 300\varepsilon^p$ and shows that inter-element discontinuities do not pollute the stress integration. The difference between the predicted and the actual hardening is significantly lower than the reported scatter for this benchmark in the literature [7, 23] and hence the mechanical soundness of the framework is demonstrated in the elastoplastic regime.

The local-support nature of the NURBS basis is reflected in the 90% reduction in the geometric DOF (100 vs. 1000 control points, MSE = 4.23 vs. 0.21 mm^2). This is a geometric economy, which is preserved in the hybrid framework, and is beneficial for large-scale structural analysis.

The following limitations of the present study should be noted explicitly. First, the formulation is restricted to single patch cylindrical geometries. For multi-patch configurations the Hermite–NURBS coupling conditions must be compatible at patch boundaries, a non-trivial task because the derivative DOF at one patch boundary must be consistently mapped onto the adjacent patch parameterization. Nitsche-type or mortar methods might provide viable ways and this is being developed. Second, there are only two benchmark problems that are studied: a linear elastic Scordelis–Lo roof and an elastoplastic pinched cylinder. Dynamic loading (impact, vibration), thermal gradients and cyclic plasticity tests have not been done yet. Third, although the hybrid framework works well for the benchmarks studied, there are no formal a priori error estimates available for the anisotropic Hermite×NURBS tensor product. The problem of deriving such estimates is an important open theoretical problem, especially the convergence rates as functions of the axial Hermite order and circumferential NURBS degree. Fourth, the conditioning of the hybrid stiffness matrix was not investigated quantitatively in the present study. Hermite-based formulations are known to generate larger condition numbers than standard displacement-based discretizations because of the presence of derivative degrees of freedom. Nevertheless, no convergence difficulties, numerical instabilities, or solver failures were observed in any of the benchmark problems considered. A systematic investigation of condition numbers, iterative solver performance, and suitable preconditioning strategies remains an important topic for future research. Fifth, the hybrid framework is developed for anisotropic refinement scenarios and is not recommended as a general replacement for NURBS-IGA, which remains more DOF-efficient for isotropic refinement; the choice should therefore be based on the structural geometry and refinement requirements. Multi-patch coupling, extension to doubly-curved shells and stiffened panels, composite and functionally graded materials, and the derivation of a posteriori error estimators for adaptive hybrid refinement will be investigated in future work.

8. Conclusion

This work has presented a hybrid Hermite×NURBS Kirchhoff–Love shell formulation that addresses two principal limitations of many existing KL shell formulations. It maintains the exact geometry of NURBS in the circumferential direction while enforcing C^1 continuity in the axial direction using cubic Hermite interpolation without global knot propagation. The hybrid discretization method shows a monotonically converging solution to the reference solution on the Scordelis–Lo benchmark, with an error of 0.02% at 3900 DOF, and an empirical convergence rate of about 5. This behavior is attributed to the significant mitigation of membrane locking effects through the exact NURBS representation of the circumferential geometry. This behavior is verified by the study of the L^2 norm and H^1 norm (Section 5.3), which demonstrate the monotone convergence of the displacement field at an empirical order of about 2.3.

Author Contributions

H. Outaybi contributed to the conceptualization, methodology, software development, formal analysis, and preparation of the original draft of the manuscript. J. El-Mekkaoui was responsible for validation, investigation, and manuscript review and editing. A.

El Khalfi supervised the study and contributed to the review and editing of the manuscript. M. Luminita Scutaru and S. Vlase contributed to the review and editing of the manuscript. All authors read and approved the final published version of the manuscript.

Acknowledgments

Not applicable.

Conflict of Interest

The authors declare no conflict of interest.

Funding

Not applicable.

Data Availability Statements

The Python and MATLAB source codes are available from the corresponding author upon reasonable request.

Nomenclature

NURBS	Non-Uniform rational B-Splines
CAD	Computer-Aided design
FEM	Finite element method
IGA	Isogeometric analysis
KL	Kirchhoff–Love (shell theory)
RM	Reissner–Mindlin (shell theory)
DOF	Degrees of freedom
MSE	Mean squared error
PEEQ	Equivalent plastic strain
E	Young's modulus [N/mm²]
ν	Poisson's ratio
ε^p	Equivalent plastic strain
$h(\varepsilon^p)$	Hardening law: $h(\varepsilon^p) = 24.3 + 300\varepsilon^p$ [N/mm²]
ξ, η, ζ	Parametric coordinates
$N_{i,p}(\xi)$	B-spline basis function of degree p
$R_{i,p}(\xi)$	NURBS rational basis function
w_i	Weight associated with control point i
p, q, r	Polynomial degrees in ξ, η, ζ directions
C^0, C^1	Positional / first-order continuity
K^e	Element stiffness matrix

References

[1] Hughes, T.J.R., Cottrell, J.A., Bazilevs, Y., Isogeometric analysis: CAD, finite elements, NURBS, exact geometry, and mesh refinement, *Computer Methods in Applied Mechanics and Engineering*, 194, 2005, 4135-4195.

[2] Kiendl, J., Bletzinger, K.-U., Linhard, J., Wüchner, R., Isogeometric shell analysis with Kirchhoff–Love elements, *Computer Methods in Applied Mechanics and Engineering*, 198, 2009, 3902-3914.

[3] Kim, M.G., Lee, G.H., Lee, H., Koo, B., Isogeometric analysis for geometrically exact shell elements using Bézier extraction of NURBS with assumed natural strain method, *Thin-Walled Structures*, 172, 2022, 108846.

[4] Liu, C., Tian, Q., Hu, H., New spatial curved beam and cylindrical shell elements, *Nonlinear Dynamics*, 70, 2012, 1903-1918.

[5] Matikainen, M.K., Mikkola, A., Schwab, A.L., The quadrilateral fully-parametrized plate elements based on the absolute nodal coordinate formulation, *Journal of Structural Mechanics*, 42, 2009, 138-148.

[6] Ambati, M., Kiendl, J., De Lorenzis, L., Isogeometric Kirchhoff–Love shell formulation for elasto-plasticity, *Computer Methods in Applied Mechanics and Engineering*, 340, 2018, 320-339.

[7] Guo, M., Wang, W., Zhao, G., Du, X., Zhang, R., Yang, J., T-splines for isogeometric analysis of the large deformation of elastoplastic Kirchhoff–Love shells, *Applied Sciences*, 13, 2023, 1709.

[8] Cottrell, J.A., Hughes, T.J.R., Bazilevs, Y., Isogeometric Analysis: Toward Integration of CAD and FEA, *Wiley*, 2009.

[9] Casquero, H., Liu, L., Zhang, Y., Reali, A., Kiendl, J., Gomez, H., Arbitrary-degree T-splines for isogeometric analysis of fully nonlinear Kirchhoff–Love shells, *Computer-Aided Design*, 82, 2017, 140-153.

[10] Coradello, L., D'Angelo, P., Vázquez, R., Buffa, A., Adaptive isogeometric analysis on two-dimensional trimmed domains based on a hierarchical approach, *Computer Methods in Applied Mechanics and Engineering,* 380, 2021, 113782.

[11] Hirschler, T., Bouclier, R., Duval, A., Elguedj, T., Morlier, J., The embedded isogeometric Kirchhoff–Love shell: From design to shape optimization of non-conforming stiffened multipatch structures, *Computer Methods in Applied Mechanics and Engineering*, 349, 2019, 774-797.

[12] Liu, C., Wang, S., Xie, X., Adaptive isogeometric topology optimization of shell structures based on truncated hierarchical B-splines, *Frontiers of Mechanical Engineering*, 20(6), 2025, 49.

[13] Rabczuk, T., Areias, P.M.A., A meshfree thin shell for arbitrary evolving cracks based on an extrinsic basis, *CMES-Computer Modeling in Engineering & Sciences*, 8, 2006, 115-130.

[14] Rabczuk, T., Areias, P.M.A., Belytschko, T., A meshfree thin shell method for nonlinear dynamic fracture, *International Journal for Numerical Methods in Engineering*, 72, 2007, 524-548.

[15] Nguyen-Thanh, N., Nguyen-Xuan, H., Bordas, S., Rabczuk, T., Isogeometric analysis using polynomial splines over hierarchical T-meshes for two-dimensional elastic solids, *Computer Methods in Applied Mechanics and Engineering,* 200, 2011, 1892-1908.

[16] Samaniego, E., Anitescu, C., Goswami, S., Nguyen-Thanh, V.M., Guo, H., Hamdia, K., Zhuang, X., Rabczuk, T., An energy approach to the solution of partial differential equations in computational mechanics via machine learning, *Computer Methods in Applied Mechanics and Engineering*, 362, 2020, 112790.

[17] Nguyen-Thanh, V.M., Anitescu, C., Alajlan, N., Rabczuk, T., Zhuang, X., Parametric deep energy approach for elasticity accounting for strain gradient effects, *European Journal of Mechanics - A/Solids*, 87, 2021, 104225.
[18] Petera, J., Pittman, J.F.T., Isoparametric Hermite elements, *International Journal for Numerical Methods in Engineering*, 37, 1994, 3489-3519.
[19] Attia, S., Mohareb, M., Adeeb, S., Nonlinear finite element formulation for thin-walled conical shells using Hermitian interpolation and Kirchhoff–Love kinematics, *Thin-Walled Structures*, 205, 2024, 112617.
[20] Oumellal, F., Lamnii, A., Curve and surface construction using Hermite trigonometric interpolant, *Mathematical and Computational Applications*, 26, 2021, 11.
[21] Riffnaller-Schiefer, A., Augsdörfer, U.H., Fellner, D.W., Isogeometric shell analysis with NURBS compatible subdivision surfaces, *Applied Mathematics and Computation*, 272, 2016, 139-147.
[22] Brank, B., Perić, D., On large deformations of thin elastoplastic shells, *International Journal for Numerical Methods in Engineering*, 40, 1997, 689-726.
[23] Areias, P.M.A., Ritto-Corrêa, M.C., Martins, J.A.C., Finite strain plasticity, the stress condition, and a complete shell model, *Computational Mechanics*, 45, 2010, 189-209.
[24] Piegl, L., Tiller, W., *The NURBS Book*, 2nd ed., Springer, 1997.
[25] Krysl, P., Chen, J.-S., Benchmarking computational shell models, *Archives of Computational Methods in Engineering*, 30, 2023, 301-315.
[26] Belytschko, T., Stolarski, H., Liu, W.K., Carpenter, N., Ong, J.S.J., Stress projection for membrane and shear locking in shell finite elements, *Computer Methods in Applied Mechanics and Engineering*, 51, 1985, 221-258.
[27] Riks, E., An incremental approach to the solution of snapping and buckling problems, *International Journal of Solids and Structures*, 7, 1979, 529-551.
[28] Cortivo, N.D., Felippa, C.A., Bavestrello, H., Silva, W.T.M., Plastic buckling and collapse of thin shell structures, *Computer Methods in Applied Mechanics and Engineering*, 198, 2009, 785-798.
[29] MacNeal, R.H., Harder, R.L., A proposed standard set of problems to test finite element accuracy, *Finite Elements in Analysis and Design*, 1, 1985, 3-20.
[30] Veldin, T., Brank, B., Brojan, M., Discrete Kirchhoff–Love four-node shell finite element based on the Hermite interpolation and membrane locking treatment, *Thin-Walled Structures*, 168, 2021, 108268.
[31] Tornabene, F., Viscoti, M., Dimitri, R., Higher-order weak formulation for vibration analysis of anisotropic doubly-curved shells, *Engineering Analysis with Boundary Elements*, 180, 2025, 106480.
[32] Hermite, C., Sur quelques formules relatives à l'interpolation, *Journal de Mathématiques Pures et Appliquées*, 6, 1869, 1-10.

ORCID iD

Hajar Outaybi https://orcid.org/0009-0000-6093-4663
Jaouad El-Mekkaoui https://orcid.org/0000-0002-9209-7086
Ahmed El Khalfi https://orcid.org/0000-0001-9861-8316
Maria Luminita Scutaru https://orcid.org/0000-0002-0132-1282
Sorin Vlase https://orcid.org/0000-0001-8679-2579

How to cite this article: Outaybi H. et al., Directional C¹ Continuity Without Global Knot Propagation in Kirchhoff–Love Shells: A Hermite–NURBS Strategy for Membrane Locking Reduction and Elastoplastic Validation, *J. Appl. Comput. Mech.*, xx(x), 2026, 1–12. https://doi.org/10.22055/jacm.2026.49288.5869